

Integrating Pure Pixel Identification into Nonnegative Matrix Factorization for Endmember Extraction

Huadong Yang, Nan Xu, and Yongping Hao

Abstract—Hyperspectral unmixing (HU) has been widely used to address the mixed-pixel problem in the quantitative analysis of hyperspectral remote sensing images, in which endmember extraction plays a very important role. In this paper, a two-stage algorithm is presented for endmember extraction. The first stage aims at finding pure endmembers that have pure pixel representations in the hyperspectral scene. At first, pure-pixel-based endmember extraction algorithms are exploited to find the spectrally pure pixels directly from hyperspectral images as initial pure pixel candidates, and then local spatial-spectral information is utilized to determine pure endmembers. The second stage aims at generating virtual endmembers (not necessarily present in the set comprised by input data samples). We extend the original nonnegative matrix factorization (NMF) unmixing model to incorporate endmember *a priori* information, and then use the extended NMF method to generate virtual endmembers. Experimental results with both simulated and real hyperspectral data sets have validated the effectiveness of our method and have demonstrated that the known endmember information is beneficial to the extraction of other unknown endmembers.

Index Terms—Hyperspectral unmixing, endmember extraction, spatial information, nonnegative matrix factorization

I. INTRODUCTION

HYPERSPECTRAL imaging has become one of the most powerful and fastest growing technique in remote sensing. Its benefits and advantages come from its use of as many as hundreds of narrow and contiguous spectral bands from the visible region through the infrared region. However, because of the limited spatial resolution of the sensors, e.g., NASA's Airborne Visible/ Infrared Imaging Spectrometer (AVIRIS) has 20-m ground resolution when flown at high altitude (20km), more than one type of material can be present in a single pixel, these pixels are called mixed pixels, whereas pixels with only one type of material present are called pure pixels. The wide existence of mixed pixels is a common

problem associated with hyperspectral images [1], which makes it hard to apply the traditional pixel level methods in certain domains such as identification and detection of ground targets. Hyperspectral unmixing (HU) is a key technique of mixed pixel processing, it aims to decompose the mixed pixel into a set of pure constituent spectra (called *endmembers* signatures) and their corresponding fractional abundances [2]. HU involves two steps: endmember extraction and abundance estimation. Endmember extraction aims to identify the endmember signatures from hyperspectral data, and abundance estimation aims to infer the proportions of different endmembers in forming each pixel. Endmember extraction is a very challenging task due to the intrinsic complexity of remote sensing images and the lack of priori knowledge.

In recent years, a number of endmember extraction methods have been developed, where many of them search for distinctive image pixels from hyperspectral scene as endmember signatures. These method usually implicitly assume that the input hyperspectral data set contains at least one pure pixel for each distinct material present in the scene. Therefore, a search procedure aimed at finding the most spectrally pure signatures in the input scene is feasible. Techniques include, among many others [2], the pixel purity index (PPI) algorithm [3], the N-FINDR algorithm [4], the vertex component analysis (VCA) algorithm [5], and the simplex growing algorithm (SGA) [6]. These algorithms exploit the geometrical fact that, under the linear mixing model, the observed pixel vectors in a given scene belong to a simplex set whose vertices correspond to the endmembers. Therefore, finding the endmembers is equivalent to identify the vertices of the referred to simplex. The well-known N-FINDR algorithm is based on a criterion that the volume of simplex formed by the purest pixels is maximum, and fulfills this criterion by inflating the simplex inside the data set. The original N-FINDR algorithm is implemented in the parallel mode, and the SGA algorithm is its sequential version. PPI and VCA are to orthogonally project data samples on a set of selected vectors so that the data samples whose orthogonal projections fall at the end (extreme) points of these selected vectors will be considered as endmember candidates.

Although the pure-pixel-based algorithms have been quite successful when pure pixel are present in the original hyperspectral image, for the case of highly mixed data, this assumption may be seriously violated. In order to deal with this important issue, other methods have been proposed that do not assume the presence of pure signatures in the input data.

Manuscript received July 9, 2018; revised Oct. 21, 2018. This work was supported by the Natural Science Foundation of Liaoning Province under Grant 1552638292821.

Huadong Yang is with the School of Information Science and Engineering, Shenyang Ligong University, Shenyang 110159, China (e-mail: yanghd8608@gmail.com).

Nan Xu is with the BIM and Computing Technology Research Center, Shenyang Jianzhu University, Shenyang 110168, China (e-mail: xunan0424@sina.com).

Yongping Hao is with the School of Equipment Engineering, Shenyang Ligong University, Shenyang 110159, China (e-mail: yphsit@126.com).

Instead, these methods aim at generating virtual endmembers (not necessarily present in the set composed of input data samples and most likely without physically meaningful spectral signatures). Techniques in this category include volume minimization approaches inspired by minimum volume transform (MVT) algorithm [7], such as minimum volume simplex analysis (MVSA) [8], simplex identification via variable splitting and augmented Lagrangian (SISAL) [9], and the minimum-volume enclosing simplex (MVES) [10].

Nonnegative matrix factorization (NMF) based unmixing algorithm is another branch of non-pure-pixel-based algorithm. NMF was originally proposed for object recognition and has also attracted much attention [11]–[13]. It aims to decompose the observation matrix into a product of two nonnegative matrices, corresponding to the endmember matrix and abundance matrix, respectively. NMF-based techniques have no requirement for existence of pure pixels and seem to be very attractive for unmixing hyperspectral data. However, NMF is a non-convex problem that may fall into local minima and is strongly influenced by the initialization step. A typical solution is to impose the auxiliary constraints on the NMF model. Miao and Qi [14] introduced the minimum volume constraint into NMF model for unsupervised endmember extraction. Jia and Qian [15] proposed to force the smoothness of the endmember and the abundance. Wang et al. [16] set spectra signature dissimilarity as the constraint on endmembers.

Apart from the aforementioned algorithms, there is another kind of unmixing algorithm that takes both spectral and spatial information into account to improve the quality of extracted endmembers, such as the automatic morphological endmember extraction (AMEE) algorithm [17], the spatial-spectral endmember extraction (SSEE) algorithm [18], the spatial purity based endmember extraction (SPEE) algorithm [19], the superpixel endmember detection algorithm [20], a region-based spatial preprocessing (RBSPP) approach [21], and spatial preprocessing (SPP) using a sliding-window approach [22]. The first four approaches are endmember extraction algorithms themselves, whereas the latter two approaches are preprocessing modules that can be applied prior to any other endmember extraction algorithm.

As mentioned above, these algorithms either find pure pixels directly from remote sensing images as desired endmembers assuming the presence of at least one pure pixel of each endmember in the data or generate virtual pixels (signatures) as desired endmembers without pure-pixel assumption. However, what happens in real scene is that some widespread materials have pure pixel representations, while the other less wide-spread materials only have mixed pixel representations. Therefore, we consider integrating the pure-pixel-based methods and non-pure-pixel-based methods for improving the accuracy of endmember extraction.

In this paper, we present a novel endmember extraction algorithm, which incorporate the pure-pixel-based endmember extraction procedure into the NMF unmixing scheme, referred to as the pure pixel identification based NMF (PPI-NMF) algorithm. The proposed PPI-NMF algorithm involves two stages. The first stage aims at finding the spectrally pure pixels directly from data set. We first perform the traditional pure-pixel-based endmember

extraction algorithm to find pure pixel candidates, which contains pure pixels and/or “purest” mixed pixels. Then, local spatial information is utilized to refine the pure pixel candidates to pure endmembers. The second stage aims at producing virtual endmembers by performing the NMF-based unmixing method. In order to effectively use the extracted pure endmembers, we extend the original NMF unmixing model to incorporate endmember *a priori* information.

The remainder of this paper is organized as follows. Section II introduces the linear mixture model and NMF briefly. Section III details the proposed algorithm. Results on synthetic and real-world data are reported in Sections IV. Finally, we present our conclusion in Section V.

II. RELATED WORKS

Before giving the derivation of our proposed approach, two basic concepts, linear mixture model and nonnegative matrix factorization are first introduced in this section.

A. Linear Mixture Model (LMM)

LMM, as the simplest and most widely used model for hyperspectral data analysis, assumes that the spectral signature of an image pixel can be represented by linear mixtures of a finite number of endmembers and the linear coefficient of each endmember is its abundance. Given a hyperspectral data set with P endmembers, an observed pixel \mathbf{x} can be written as

$$\mathbf{x} = \mathbf{M}\mathbf{s} + \mathbf{e} \quad (1)$$

where \mathbf{M} is an $L \times P$ matrix ($\mathbf{m}_1, \dots, \mathbf{m}_i, \dots, \mathbf{m}_P$), in which \mathbf{m}_i is an $L \times 1$ column vector representing the spectral signature of the i th endmember. \mathbf{s} is a $P \times 1$ column vector ($s_1, \dots, s_i, \dots, s_P$)^T for abundances. The last term \mathbf{e} takes into account possible errors and sensor noises. Because spectral responses of endmembers and their abundance in each pixel cannot be smaller than zero, nonnegativity constraint (i.e., $s_i \geq 0$) is generally imposed on abundance vector \mathbf{s} . Moreover, sum-to-one constraint (i.e., $\sum_1^P s_i = 1$) are generally imposed on abundance vector \mathbf{s} for physical consideration.

Using matrix notation, the aforementioned mixing model for the N pixels in the image can be rewritten as

$$\mathbf{X} = \mathbf{M}\mathbf{S} + \mathbf{E} \quad (2)$$

where matrices $\mathbf{X} \in R^{L \times N}$, $\mathbf{S} \in R^{P \times N}$, and $\mathbf{E} \in R^{L \times N}$ represent the hyperspectral image, the abundance matrix and the error matrix, respectively.

B. Nonnegative Matrix Factorization

NMF is a matrix factorization algorithm that focuses on the analysis of data matrices whose elements are nonnegative. Given a nonnegative matrix $\mathbf{X} \in R^{L \times N}$, NMF aims to find two nonnegative matrices $\mathbf{M} \in R^{L \times P}$ and $\mathbf{S} \in R^{P \times N}$ whose product can well approximate the original matrix \mathbf{X} :

$$\mathbf{X} \approx \mathbf{M}\mathbf{S} \quad (3)$$

A comparison between models in (2) and (3) clearly shows the potential of applying NMF to a HU problem.

One natural way to solve the NMF problem is to formulate an optimization problem by minimizing the Euclidean distance between \mathbf{X} and $\mathbf{M}\mathbf{S}$ (i.e., the difference between hyperspectral image data \mathbf{X} and the reconstructed image $\mathbf{M}\mathbf{S}$).

Therefore, an objective function can be defined as follows

$$\min_{\mathbf{M}, \mathbf{S}} f(\mathbf{M}, \mathbf{S}) = \frac{1}{2} \|\mathbf{X} - \mathbf{MS}\|_F^2 \quad (4)$$

where $\|\cdot\|$ represents the Frobenius norm.

Although the minimization problem is convex in \mathbf{M} and \mathbf{S} separately, it is not convex in both simultaneously. In order to minimize it, Lee and Seung developed multiplicative update rules that are guaranteed to converge to local optima under the nonnegative constraints of two factorized matrices [13]. In this paper, we also use the multiplicative update rules for the NMF unmixings of \mathbf{X} , which are given as follows:

$$\mathbf{M} \leftarrow \mathbf{M} \cdot \mathbf{XS}^T / \mathbf{MSS}^T \quad (5)$$

$$\mathbf{S} \leftarrow \mathbf{S} \cdot \mathbf{M}^T \mathbf{X} / \mathbf{M}^T \mathbf{MS} \quad (6)$$

where $(\cdot)^T$ is the transpose of the matrix, “ \cdot ” and “ \cdot ” are MATLAB notations, representing elementwise matrix multiplication and division, respectively.

III. THE PROPOSED METHOD

Based on the analysis mentioned in Section I, the proposed PPI-NMF algorithm can be divided into the following steps: 1) identifying pure endmembers by performing traditional pure-pixel-based endmember extraction algorithm with spatial information; 2) generating virtual endmembers by the modified NMF algorithm.

A. Identifying Pure Endmembers

The pure-pixel-based endmember extraction algorithm aims to identify the spectrally pure pixels as the endmembers and performs well for the case of presence of pure signatures. When some of endmembers do not have pure pixel representations, it only finds the “purest” mixed pixels available in the scene as desired endmembers. This is to say that the endmembers extracted by pure-pixel-based endmember extraction algorithm contain both pure and mixed pixels, leading to degenerate the accuracy of endmembers.

As shown in the spatial-spectral endmember extraction algorithm [17]–[22], spatial information can be used as a guide to effectively identify spectrally pure pixels. Generally, pure pixels are more likely to be present in spatially homogeneous areas, and the variance of pixels presented in the homogenous area is very small. In other words, if a candidate pixel locate in a homogeneous area covered by only one type material, it can be select as the pure endmembers for endmember extraction.

With the aforementioned design principle in mind, in this work we develop a pure pixels identification scheme which integrates spatial and spectral information into the process of endmember extraction.

The first step is to obtain the initial pure pixel candidates. This task is fulfilled using pure-pixel-based endmember extraction algorithms, such as PPI, VCA, NFINDR, and SGA. It should be noted, however, that the final sets of endmembers produced by first three algorithms in different runs are usually not consistent. One possible solution is to run the algorithm many times and choose the pure candidates according to their frequency of occurrence.

The second step aims to identify pure endmembers from the initial pixel candidates obtained in the first step. As mentioned above, the spectral signatures of pixels from

homogeneous ground objects presenting in adjacent areas are very similar, and vice versa. Therefore, whether a pixel locates at the spatially homogeneous area can be judged by the spectral similarity between itself and its spatial adjacent pixels inside the region delimited by the window with a size of $k \times k$ pixels.

Several pointwise distances metric can be considered in order to compute the spectral similarity. In this paper, we have used the spectral angle distance (SAD) [1], which is a well-known metric for hyperspectral data processing. SAD can be used to measure the spectral similarity between two pixel vectors as follows:

$$\text{SAD}(\mathbf{x}_i, \mathbf{x}_j) = \arccos \frac{\mathbf{x}_i \cdot \mathbf{x}_j}{\|\mathbf{x}_i\| \|\mathbf{x}_j\|} \quad (7)$$

where \mathbf{x}_i and \mathbf{x}_j are two spectral vectors. It should be noted that SAD is given by the spectral angle formed by n -dimensional vectors (in radians). The low SAD scores mean high spectral similarity between the compared vectors. Therefore, we consider that the pixel locates at the spatially homogeneous area when the SAD of the pixel and its neighbors is less than the given threshold θ .

In the final step, principal component analysis (PCA) is performed on homogeneous areas to discriminate pure from mixed. In general, if the homogenous pixels are pure, i.e., only one endmember exists in the homogenous area, the first principal component will be the dominant component whereas the other principal components come as a result of local spectral variability. Therefore, the first eigenvalue is much greater than the other eigenvalues. On the contrary, when the homogenous pixels are mixed, there exists more than one dominant component corresponding to several ground objects. As a consequence, pure homogeneous area can be determined in terms of the variance ratio contribution of the first principal component.

Suppose \mathbf{C} is the covariance matrix of mean-subtracted pixels in a homogenous area, the PCA of the spectra data can be denoted as follows:

$$[\mathbf{E}, \mathbf{D}] = \text{PCA}(\mathbf{C}) \quad (8)$$

where \mathbf{D} is a diagonal matrix whose diagonal elements are the eigenvalues of \mathbf{C} sorted in descending order and \mathbf{E} correspond to their eigenvectors. Assume there are k eigenvalues in the PCA of a homogeneous area, the variance ratio contribution of the first principal component (denoted by vrc) can be described as follows:

$$vrc = \frac{d_{11}}{\sum_{i=1}^k d_{ii}} \quad (9)$$

where d_{ii} is the i th eigenvalue.

According to the vrc defined in (9), the variance ratio contribution of the first principal component of pure and mixed homogeneous area obtained by pure-pixel-based endmember extraction algorithms have significant differences. Therefore, it is much easier to set the threshold and to determine pure endmembers by comparing the variance ratio contribution of the first principal component with the predefined threshold. In order to reduce the effects of noise and to average out the subtle spectral variability of a given class, pure homogeneous pixels are averaged to produce the final endmembers.

B. Generating Virtual Endmembers

In this section, NMF framework is used to generate virtual endmembers which only have mixed pixel representations. Since pure endmembers have been extracted, we can expect to obtain better endmember extraction results by using such endmembers information for hyperspectral unmixing. In order to accomplish this goal, we extend the original NMF model to incorporate the endmember *a priori* information.

(1) Cost Function

We assume that p pure endmembers have been extracted in the process of pure endmember identification. To make full use these pure endmembers, we add a regularizer into NMF model. Suppose $\mathbf{U} = [\mathbf{u}_1, \dots, \mathbf{u}_p, \mathbf{0}, \dots, \mathbf{0}]$ is an $L \times P$ matrix whose first p columns denote the pure endmember vectors and the rest of them are $(P - p)$ zero column vectors. Then, we propose to solve the following optimization problem:

$$\min_{\mathbf{M}, \mathbf{S}} f(\mathbf{M}, \mathbf{S}) = \frac{1}{2} \|\mathbf{X} - \mathbf{M}\mathbf{S}\|_F^2 + \frac{1}{2} \lambda \|\mathbf{U} - \mathbf{M}\mathbf{Q}\|_F^2 \quad (10)$$

s.t. $\mathbf{M} \geq 0, \mathbf{S} \geq 0$

where $\lambda \geq 0$ is a regularization parameter which weights the contribution of the pure endmembers, and \mathbf{Q} is a $P \times P$ matrix defined as follows:

$$\mathbf{Q} = \begin{bmatrix} \mathbf{I} & \mathbf{0} \\ \mathbf{0} & \mathbf{0} \end{bmatrix} \quad (11)$$

where \mathbf{I} is the $p \times p$ identity matrix.

The first term in (10) is the same as the reconstruction error in the NMF model in (4). The second term (i.e., regularizer) is proposed to make full use of the known endmembers information. In practical applications, if we confirm that some materials in the spectral library are known to exist in the hyperspectral scene, the matrix \mathbf{U} in second term can be directly constructed using spectral signatures in the library.

(2) The Update Rules

To solve the formulated optimization problem, we adopt the multiplicative update rule stated in [12]. When applied to (9), the update rules of our proposed approach can be formulated as follows:

$$\mathbf{M} \leftarrow \mathbf{M} \cdot \frac{(\mathbf{X}\mathbf{S}^T + \lambda\mathbf{U}\mathbf{Q}^T)}{(\mathbf{M}\mathbf{S}\mathbf{S}^T + \mathbf{M}\mathbf{Q}\mathbf{Q}^T)} \quad (12)$$

$$\mathbf{S} \leftarrow \mathbf{S} \cdot \frac{\mathbf{M}^T \mathbf{X}}{\mathbf{M}^T \mathbf{M}\mathbf{S}} \quad (13)$$

In order to take care of sum-to-one constraint, we adopt a simple but effective method stated in [23]. We augment the data matrix \mathbf{X} and the endmember matrix \mathbf{M} by a row of constant denoted by

$$\bar{\mathbf{X}} = \begin{bmatrix} \mathbf{X} \\ \delta \mathbf{1}_N^T \end{bmatrix}, \quad \bar{\mathbf{M}} = \begin{bmatrix} \mathbf{M} \\ \delta \mathbf{1}_P^T \end{bmatrix} \quad (14)$$

where $\mathbf{1}_N$ ($\mathbf{1}_P$) is a N (P)-dimensional column vector of all 1s, and δ is a positive number to control the effect of the sum-to-one constraint on the abundance matrix \mathbf{S} . As δ increases, the columns of \mathbf{S} are forced to approach the sum-to-one constraint. In our experiments, we set δ to 10.

(3) The Initialization and Stopping Conditions

The initialization of the NMF procedure for unmixing can seriously affect the accuracy of the results. In this paper, VCA method [5] is used to generate the initial endmember matrix. After that, the initialization of the abundance matrix is estimated by the well-known fully constrained least square (FCLS) spectral unmixing algorithm [23].

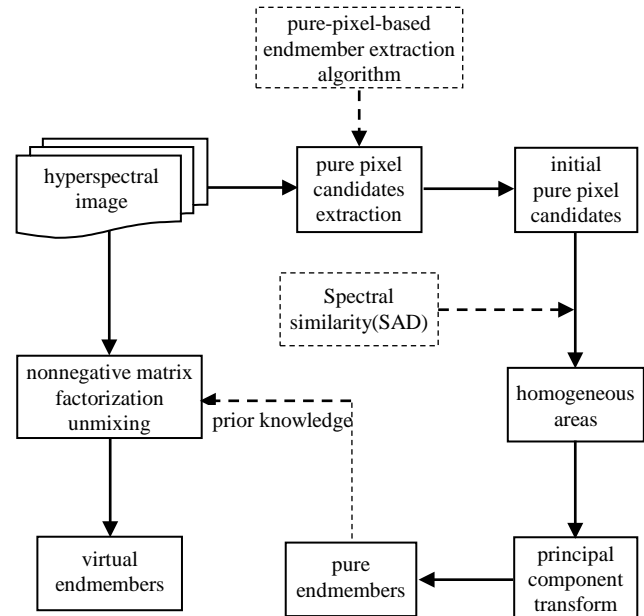


Fig. 1. Flowchart of the proposed PPI-NMF method.

The procedure of NMF should be stopped when a stationary point is reached. Two stopping criteria are used in our implementation. The first one is the maximum iteration number which is set to 1000. The second one is the gradient difference of the objective function between the current and the previous iterations:

$$|f(\mathbf{M}^i, \mathbf{S}^i)| \leq \varepsilon |f(\mathbf{M}^{i-1}, \mathbf{S}^{i-1})| \quad (15)$$

where ε is set to 10^{-4} in the experiments. Once either of these criteria is met, the optimization process terminates.

(4) The process of the constrained NMF algorithm

Based on the above statement and analysis, the procedure of the proposed NMF algorithm is summarized as follows.

Algorithm 1:

Data: Hyperspectral image \mathbf{X}

Initialization: Endmember matrix \mathbf{M} , abundance matrix \mathbf{S} , known endmember matrix \mathbf{U} and auxiliary matrix \mathbf{Q} .

while stop conditions are not met **do**

1. Augment \mathbf{X} and \mathbf{M} to $\bar{\mathbf{X}}$ and $\bar{\mathbf{M}}$;

2. Update \mathbf{M} by Equation (12);

3. Update \mathbf{S} by Equation (13).

end

Output: \mathbf{M} and \mathbf{S}

C. The Proposed PPI-NMF Algorithm

Based on the proposed pure pixel identification algorithm and the constrained NMF algorithm, a general flowchart of PPI-NMF is depicted in Fig.1. The input of the PPI-NMF algorithm is the whole hyperspectral image. At first, pure-pixel-based endmember extraction algorithm are performed to find the spectrally pure pixels as initial pure pixel candidates. Since the initial pure pixel candidates may contain both pure and mixed pixels, the spectral angle distance and principal component transform are then utilized to discriminate the pure from mixed in the candidate set, and these pure pixels are selected as the pure endmembers. Finally, a constrained NMF algorithm with pure endmember information is performed to generate the virtual endmembers.

IV. EXPERIMENTS AND ANALYSIS

In order to validate the proposed PPI-NMF algorithm, a number of experiments were performed on synthetic data as well as the real hyperspectral data. We also compared it against several baseline HU algorithms, including VCA, SGA, SISAL and MVC-NMF. Since VCA, SGA, and SISAL are only designed for endmember extraction, which cannot estimate the abundances, FCLS is adopted to infer the abundance fractions. In the following, the combined process of VCA (SGA and SISAL) and FCLS are referred to as VCA+FCLS (SGA+FCLS and SISAL+FCLS). For our proposed PPI-NMF algorithm and MVC-NMF, SGA and FCLS are used to obtain initial endmember matrix and abundance matrix respectively. In addition, VCA and SGA algorithms are used to obtain initial pure pixel candidates in PPI-NMF algorithm, and the corresponding algorithms are marked as PPI-NMF (VCA) and PPI-NMF (SGA).

In the experiments, two metrics are used to evaluate the performance of different methods. The first metric is SAD, which is defined in (7), it is usually adopted to evaluate the similarity between true and extracted endmembers. The second metric used in this work is the root mean square error (RMSE) between the original and a reconstructed version of the hyperspectral scene. The RMSE is often used to compare the accuracy of the abundance estimation. It is defined as follows:

$$\text{RMSE}_i = \left(\frac{1}{N} \|\hat{\mathbf{S}}_i - \mathbf{S}_i\|^2 \right)^{\frac{1}{2}} \quad (15)$$

where $\hat{\mathbf{S}}_i$ is the reference abundance matrix for i th endmember. Generally speaking, the smaller the RMSE is, the more the estimation approximates the truth.

A. Experiments with Synthetic Data

We first evaluate and analyze the proposed method on synthetic data. To generate the synthetic data, a set of spectral signatures are chosen from the United States Geological Survey (USGS) digital spectral library [24]. The selection of endmember signatures is arbitrary as long as they are linearly independent. To simulate possible errors and sensor noise, zero-mean Gaussian noise is added to synthetic data. The signal-to-noise ratio (SNR) is defined as

$$\text{SNR} = 10 \log_{10} \frac{E(\mathbf{x}^T \mathbf{x})}{E(\boldsymbol{\varepsilon}^T \boldsymbol{\varepsilon})} \quad (16)$$

where $\boldsymbol{\varepsilon}$ is the noise vector, and $E(\cdot)$ stand for mathematical expectation operator. The default setting of SNR is 30 on the synthetic data.

The synthetic image was generated in a similar way as in [14] through the following procedure.

- (1). The synthetic image contains 64×64 pixels, which is divided into units of 8×8 small panels. The pixels within each panel are pure and have the same type of ground cover, randomly selected as one of the endmember signatures.
- (2). Fifty dB zero-mean Gaussian noises are added to the pixels in each panel to simulate local spectral variability.
- (3). A simple 9×9 low-pass filter is used to generate mixed data.
- (4). $(8 - p)$ spectral signatures are chosen as the virtual endmember signatures. To remove pure pixels, we replace all the pixels in which abundances of the virtual

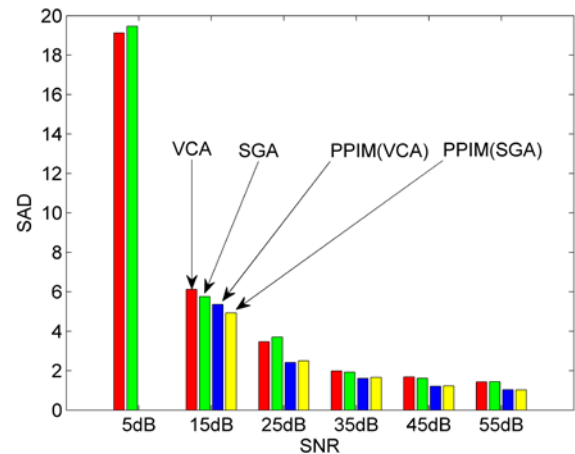


Fig. 2. SAD-based spectral similarity scores between extracted endmembers and ground-truth USGS signatures in the first experiment.

endmembers are larger than the given mixing level (denoted by *purity*, which is the highest abundance of the virtual endmembers) with a mixture made up of all endmembers of equal abundances.

- (5). Zero-mean Gaussian noises are added to the whole image to simulate contributions from ambient and instrumental sources.

In all the experiments, the parameters of PPI-NMF are set as $\theta = 3$, $k = 5$ and $\lambda = 30$. The parameters in all the other methods implemented in this paper follow their original work.

Experiment 1: The first experiment aims to validate the effectiveness of the proposed pure pixel identification method (hereafter called PPIM). As stated above, PPIM is to identify the pure endmember signatures. Accordingly, the performance of PPIM is investigated by comparing with two pure-pixel-based endmember extraction algorithms (VCA and SGA). In the experiment, synthetic scene contains eight endmembers, including six pure endmembers and two virtual endmembers. The *purity* is fixed to 0.8. The SNR is changed from 5 to 55 dB with 10dB in steps (SNR = 5, 15, ..., 55 dB). Two parameters θ and k are set to 3 and 5, respectively. In the experiment, we only compare the SADs between the reference signatures and the endmembers which have pure pixel representations in synthetic image. Since VCA generally produces different sets of final endmembers at separate runs, we run VCA algorithm 50 times and choose the ones which have the lowest SADs with reference signatures.

Fig. 2 shows the average SAD (in degrees) between the reference USGS mineral spectra and their corresponding endmember pixels produced by VCA (red color in the figure), SGA (green), PPIM with VCA (blue), and PPIM with SGA (yellow) at different noise levels. As observed from Fig. 2, the performance of all endmember extraction algorithms degrade as the noise level increases. When SNR takes higher values ($\text{SNR} \geq 15\text{dB}$), the proposed PPIM algorithm can identify the six pure pixels and match well with reference spectra, and shows the best performance overall. In addition, PPIM with VCA and PPIM with SGA outperform the VCA and SGA, respectively. At this point, it should be noted that the PPIM could not identify the pure endmembers when $\text{SNR} = 5\text{dB}$.

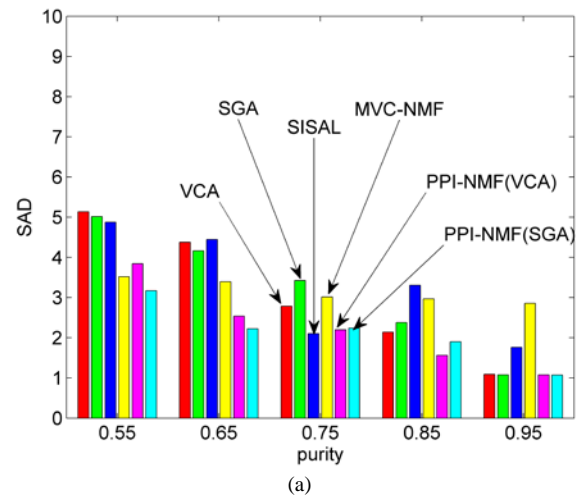
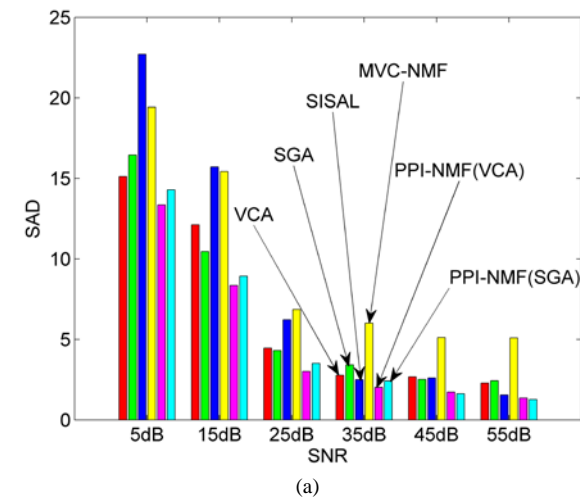


Fig. 3. Experiment results with different SNR. (a) SAD. (b) RMSE

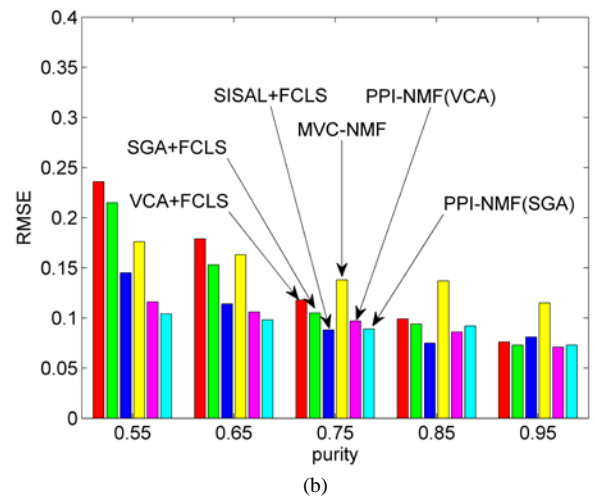


Fig. 4. Experiment results with different mixing levels. (a) SAD. (b) RMSE

This is mainly due to the fact that PPIM could not find the pure homogenous area in such worse condition. However, such low values of SNR are not often encountered in practice. On the other hand, as the case of SNR = 5 shown from Fig. 2, the average SAD values between true endmembers and estimated endmembers produced by VCA and SGA are very high. In other words, these estimated endmembers could be far away from the true endmembers, and cannot be applied in practice. As a result, we can conclude that PPIM has the potential to identify the pure endmember in different noise conditions.

Experiment 2: The third experiment is designed to evaluate the robustness of our proposed PPI-NMF algorithm with regard to different noise levels. In synthetic scene, there are six pure endmembers and two virtual endmembers, the *purity* is fixed to 0.7. SNR is varied from 5 to 55 dB with 10dB in steps. Figs. 3(a) and (b) show the average SADs and average RMSEs between true and estimated endmembers, and between true and estimated abundances, respectively.

As expected, the performance of all the algorithms degrade as the noise level increases. It indicates that noise is an important factor to consider in unmixing tasks, as a low noise level generally leads to improved unmixing accuracy. One can also see from figures that in most cases the proposed

PPI-NMF gives the best performance in terms of both SAD and RMSE. When SNR takes lower values ($\text{SNR} \geq 25\text{dB}$), the performance of PPI-NMF is marginally better than SISAL and pure-pixel-based endmember extraction algorithms (VCA and SGA) in terms of SAD. Interestingly, although both MVC-NMF and PPI-NMF are based on the NMF framework, PPI-NMF performs better than MVC-NMF. This phenomenon occurs mainly because our proposed PPI-NMF have used the endmember *a priori* information for unmixing. This is a very important feature as it reveals that endmember *a priori* can assist NMF-based unmixing algorithms to produce more realistic unmixing results in nature.

Experiment 3: The third experiment aims to study the robustness of our proposed PPI-NMF algorithm to various mixing levels. The mixing level is controlled by the parameter *purity* in data generation. In the experiment, there are eight endmembers, including four pure endmembers and four virtual endmembers, the *purity* is varied from 0.55 to 0.95 with an interval of 0.1. SNR is set to 30 dB. Figs. 4(a) and (b) illustrate the unmixing performance with different mixing levels.

From the Fig. 4, one can observe that the proposed PPI-NMF algorithm gives the best performance in most cases.

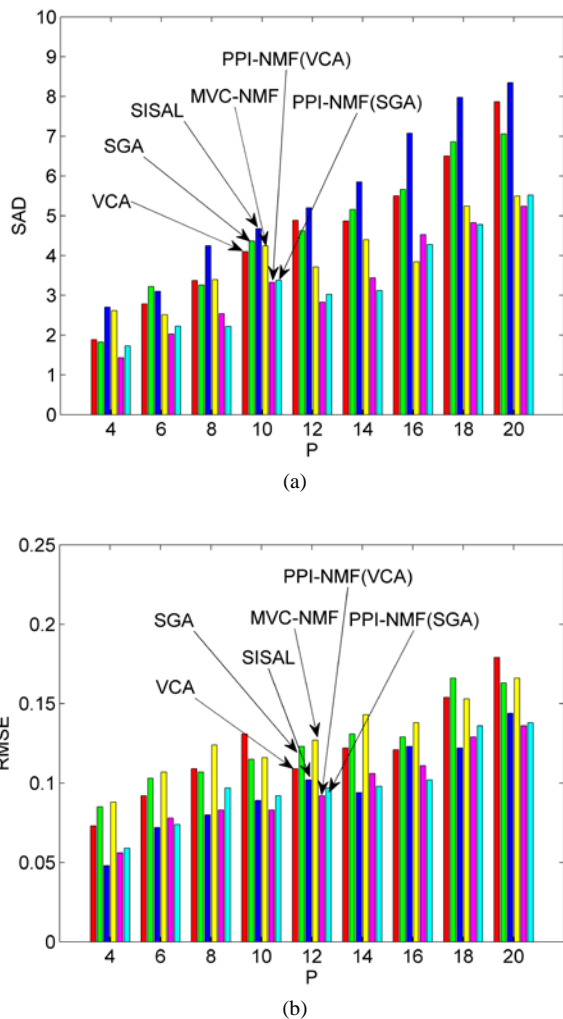


Fig. 5. Experiment results with different number of endmembers. (a) SAD. (b) RMSE

As the purity decreased, the performance of all the algorithms degrade, whereas the NMF-based unmixing algorithms (MVC-NMF and PPI-NMF) perform better than others for the case of purity < 0.75 . For higher values of purity, particularly $purity > 0.95$, almost all the endmembers have the pure pixel representations in synthetic image. This result leads to an important conclusion that PPI-NMF is not specific for unmixing highly mixed data, it can also produce reliable unmixing results when applied to hyperspectral images containing pure pixels. As the last remark, although both PPI-NMF and MVC-NMF seem to be not sensitive to the mixing level, i.e. *purity*, our proposed PPI-NMF performs better than MVC-NMF in terms of SAD and RMSE.

Experiment 4: The fourth experiment aims at testing the performance of different algorithms for synthetic data sets with different numbers of (pure and virtual) endmembers. Therefore, we created a set of synthetic scenes and changed the number of endmembers from 4 to 20 with an interval of 2. For each scene, the number of pure endmembers is equal to the number of virtual endmembers. The *purity* is fixed to 0.7, and SNR is set to 30 dB. Fig. 5(a) and (b) show the results of average SADs and average RMSEs with different number of endmembers.

As we can see from the Fig. 5 that the performance of all

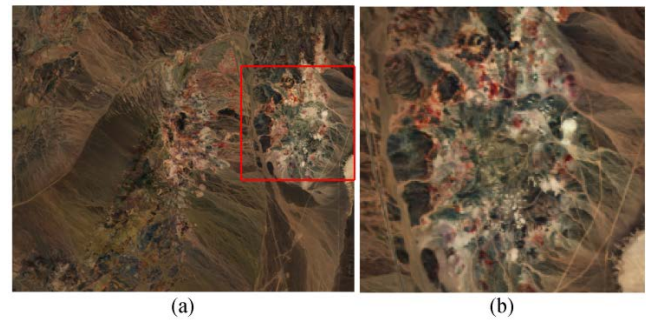


Fig. 6. Real hyperspectral image data. (a) Cuprite image acquired by AVIRIS in 1997. (b) The region of interest used in the experiment.

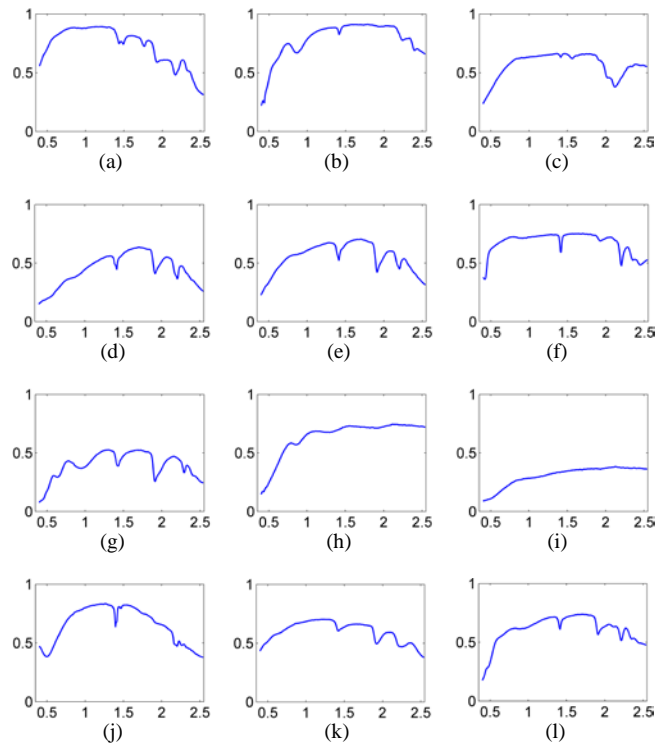


Fig. 7. Ground truth endmember signatures. (a) Alunite. (b) Andradite. (c) Buddingtonite. (d) Kaolinite1. (e) Kaolinite2. (f) Muscovite. (g) Nontronite. (h) Pyrope. (i) Sphene. (j) Dumortierite. (k) Chalcedony. (l) Montmorillonite.

algorithms degrade as the number of endmembers increased. However, in most cases, PPI-NMF performs best in terms of SAD, which is then followed by MVC-NMF, VCA and SGA, SISAL performs worst. In addition, the results shown in Fig. 5(b) demonstrate that PPI-NMF and SISAL with FCLS perform best from the abundance estimation viewpoint in terms of RMSE. In general, the experiment results indicate that incorporating the pure pixel identification procedure into NMF framework can improve unmixing accuracy once more.

B. Experiments with Real Hyperspectral Data

The real hyperspectral image data used in this experiment is the scene of the Cuprite mining district in western Nevada, USA, captured by the Airborne Visible/Infrared Imaging Spectrometer (AVIRIS) in 1997, available online in reflectance units after atmospheric correction [25]. This scene has been widely used to validate the performance of hyperspectral unmixing algorithms. This data set consists of

TABLE I
SAD BETWEEN ESTIMATED ENDMEMBERS AND REFERENCE ENDMEMBER IN
THE CUPRITE DATA.

Endmember	VCA	SGA	SISAL	MVC-NMF	PPI-NM F(VCA)	PPI-NM F(SGA)
Alunite	6.05	5.53	9.39	9.83	5.23	5.07
Andradite	4.87	5.89	5.75	8.92	8.93	5.55
Buddingtonite	8.71	10.26	7.89	11.63	7.36	7.58
Kaolinite1	7.93	6.58	8.53	9.57	9.35	10.34
Kaolinite2	12.92	13.86	12.57	14.35	8.89	9.32
Muscovite	10.93	9.17	11.69	8.49	9.04	8.87
Nontronite	16.74	17.12	10.52	11.64	10.61	12.47
Pyrope	9.79	9.91	11.64	13.33	9.67	8.76
Sphene	9.62	10.14	10.47	11.03	9.79	9.84
Dumortierite	10.37	8.26	10.61	11.18	9.03	8.33
Chalcedony	11.29	10.33	11.27	14.15	8.39	9.56
Montmorillonite	12.54	11.95	15.06	12.82	11.65	11.94
Average	10.15	9.92	10.45	11.41	9.00	8.97

224 spectral bands, with a spatial resolution of 20 m and spectral resolution of 10 nm, covering wavelength from 0.4 μ m to 2.5 μ m. In our experiment, we considered a 200 \times 200 sub-image of the hyperspectral scene as our region of interest, as shown in Fig. 6.

Prior to the analysis, several bands (1–2, 104–113, 148–167, and 221–224) were removed due to water absorption and low SNR in those bands, leaving a total of 188 reflectance channels to be used in the experiment. Since the number of endmembers must be known prior to endmember extraction, the VD [26] method was also used for this purpose. The number of endmembers is defined as 12 according to [14], and ground truth endmember signatures are shown in Fig. 7.

The SAD values between the ground truth endmember signatures and the estimated ones extracted by different unmixing algorithms are shown in Table I. For convenience of comparison, the best performance is denoted by bold font. As observed from Table I, PPI-NMF with VCA, i.e., PPI-NMF (VCA) has the highest number of best-performance cases. According to the average SAD values, PPI-NMF (SGA) slightly performs better than PPI-NMF (VCA), then followed by SGA, VCA, SISAL and MVC-NMF.

V. CONCLUSION

In this paper, we have presented a two-stage unmixing scheme which can extract both pure and virtual endmembers in real application. At first, the traditional pure-pixel-based endmember extraction algorithms are employed to search for pure pixel candidates directly from hyperspectral images. After that, the local spatial-spectral information is utilized to identify pure endmembers from pure pixel candidates. In order to make full use of the known pure endmembers, we extend the original NMF unmixing model to incorporate a prior information, and then perform it to generate virtual endmembers. The proposed method is general in nature and can be extended to other NMF-based methods with various constraints in the estimation models. A series of experiments on both synthetic and real hyperspectral data show that the proposed PPI-NMF algorithm is a promising endmember extraction algorithm.

ACKNOWLEDGMENT

The authors would like to thank Prof. C.-I. Chang, Prof. J.

M. B. Dias and Dr. L. Miao for providing the implementation code of SGA, VCA and SISAL, and MVC-NMF algorithms, respectively. The authors would also like to thank the anonymous reviewers for the many valuable comments and suggestions.

REFERENCES

- [1] N. Keshava and J. F. Mustard, "Spectral unmixing," *IEEE Signal Process. Mag.*, vol. 19, no. 1, pp. 44–57, 2002.
- [2] J. M. Bioucas-Dias, A. Plaza, N. Dobigeon, M. Parente, Q. Du, P. Gader, et al., "Hyperspectral unmixing overview: Geometrical, statistical, and sparse regression-based approaches," *IEEE J. Sel. Topics Appl. Earth Observ. Remote Sens.*, vol. 5, pp. 354–379, 2012.
- [3] J.W. Boardman, F. A. Kruse, and R. O. Green, "Mapping target signatures via partial unmixing of AVIRIS data," in *Proc. Summ. JPL Airborne Earth Sci. Workshop*, Pasadena, CA, Dec. 9–14, 1995, vol. 1, pp. 23–26.
- [4] M. E. Winter, "N-find: An algorithm for fast autonomous spectral endmember determination in hyperspectral data," in *Proc. SPIE Conf. Imaging Spectrometry V*, 1999, vol. 3753, pp. 266–275.
- [5] J. M. Nascimento and J. B. Dias, "Vertex component analysis: A fast algorithm to unmix hyperspectral data," *IEEE Trans. Geosci. Remote Sens.*, vol. 43, pp. 898–910, 2005.
- [6] C.-I. Chang, C.-C. Wu, W. Liu, and Y.-C. Ouyang, "A new growing method for simplex-based endmember extraction algorithm," *IEEE Trans. Geosci. Remote Sens.*, vol. 44, no. 10, pp. 2804–2819, 2006.
- [7] M. D. Craig, "Minimum-volume transforms for remotely sensed data," *IEEE Trans. Geosci. Remote Sens.*, vol. 32, no. 3, pp. 542–552, 1994.
- [8] J. Li and J. Bioucas-Dias, "Minimum volume simplex analysis: A fast algorithm to unmix hyperspectral data," in *Proc. IEEE Int. Geosci. Remote Sens. Symp.*, 2008, vol. 3, pp. III-250–III-253.
- [9] J. M. Bioucas-Dias, "A variable splitting augmented Lagrangian approach to linear spectral unmixing," in *Proc. 1st IEEE WHISPER*, Grenoble, France, Aug. 26–28, 2009, pp. 1–4.
- [10] T.-H. Chan, C.-Y. Chi, Y.-M. Huang, and W.-K. Ma, "A convex analysis-based minimum-volume enclosing simplex algorithm for hyperspectral unmixing," *IEEE Trans. Signal Process.*, vol. 57, no. 11, pp. 4418–4432, 2009.
- [11] D. D. Lee and H. S. Seung, "Learning the parts of objects by nonnegative matrix factorization," *Nature*, vol. 401, no. 6755, pp. 788–791, 1999.
- [12] D. D. Lee and H. S. Seung, "Algorithms for non-negative matrix factorization," in *Proc. Adv. Neural Inf. Process. Syst.*, 2000, pp. 556–562.
- [13] H. Zhuang, M. Yang, Z. Cui, and Q. Zheng, "A method for static hand gesture recognition based on non-negative matrix factorization and compressive sensing," *IAENG International Journal of Computer Science*, vol. 44, no.1, pp. 52–59, 2017.
- [14] L. Miao and H. Qi, "Endmember extraction from highly mixed data using minimum volume constrained nonnegative matrix factorization," *IEEE Trans. Geosci. Remote Sens.*, vol. 45, pp. 765–777, 2007.
- [15] S. Jia and Y. Qian, "Constrained nonnegative matrix factorization for hyperspectral unmixing," *IEEE Trans. Geosci. Remote Sens.*, vol. 47, no. 1, pp. 161–173, 2009.
- [16] N. Wang, B. Do, and L. P. Zhang, "An endmember dissimilarity constrained non-negative matrix factorization method for hyperspectral unmixing" *IEEE J. Sel. Topics Appl. Earth Observ. Remote Sens.*, vol. 6, no. 2, pp. 554–569, 2013.
- [17] A. Plaza, P. Martinez, R. Perez, and J. Plaza, "Spatial/spectral endmember extraction by multidimensional morphological operations," *IEEE Trans. Geosci. Remote Sens.*, vol. 40, no. 9, pp. 2025–2041, 2002.
- [18] D. M. Rogge, B. Rivard, J. Zhang, A. Sanchez, J. Harris, and J. Feng, "Integration of spatial-spectral information for the improved extraction of endmembers," *Remote Sens. Environ.*, vol. 110, no. 3, pp. 287–303, 2007.
- [19] S. Mei, M. He, Z. Wang, and D. Feng, "Spatial purity based endmember extraction for spectral mixture analysis," *IEEE Trans. Geosci. Remote Sens.*, vol. 48, no. 9, pp. 3434–3445, 2010.
- [20] D. R. Thompson, L. Mandrake, M. S. Gilmore and R. Castano, "Superpixel Endmember Detection," *IEEE Trans. Geosci. Remote Sens.*, vol. 48, no. 11, pp. 4023–4033, 2010.

- [21] G. Martin and A. Plaza, "Region-based spatial preprocessing for endmember extraction and spectral unmixing," *IEEE Geosci. Remote Sens. Lett.*, vol. 8, pp. 745–749, 2011.
- [22] M. Zortea and A. Plaza, "Spatial preprocessing for endmember extraction," *IEEE Trans. Geosci. Remote Sens.*, vol. 47, pp. 2679–2693, 2009.
- [23] D. C. Heinz and C.-I. Chang, "Fully constrained least squares linear spectral mixture analysis method for material quantification in hyperspectral imagery," *IEEE Trans. Geosci. Remote Sens.*, vol. 39, pp. 529–545, 2001.
- [24] R. N. Clark, G. A. Swayze, A. Gallagher, T. V. King, and W. M. Calvin, "The U.S. Geological Survey Digital Spectral Library: Version 1: 0.2 to 3.0 μm ," U.S. Geological Survey, Sunrise Valley Drive Reston, VA, Open File Rep. 93-592, 1993.
- [25] AVIRIS Data Products. [Online]. Available: <http://aviris.jpl.nasa.gov/html/aviris.freedata.html>.
- [26] C.-I. Chang and Q. Du, "Estimation of number of spectrally distinct signal sources in hyperspectral imagery," *IEEE Trans. Geosci. Remote Sens.*, vol. 42, no. 3, pp. 608–619, 2004.